RADIO OCCULTATION MEASUREMENTS WITH MARS GLOBAL SURVEYOR: DYNAMICS OF THE NEUTRAL ATMOSPHERE. D. P. Hinson, *Department of Electrical Engineering, Stanford University, 350 Serra Mall, Stanford CA 94305, dhinson@stanford.edu.*

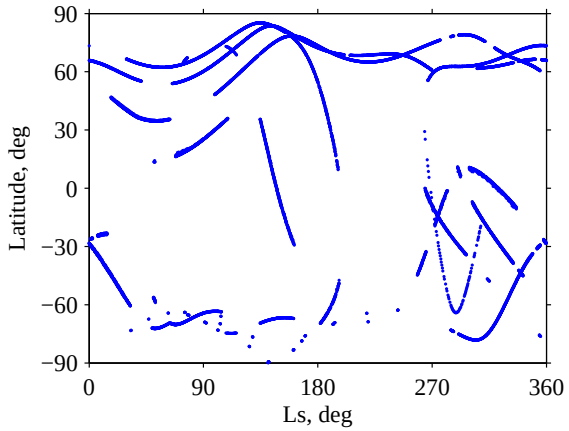

Figure 1: Coverage in latitude and season of MGS radio occultation experiments, which began in January 1998 and ended in September 2006.

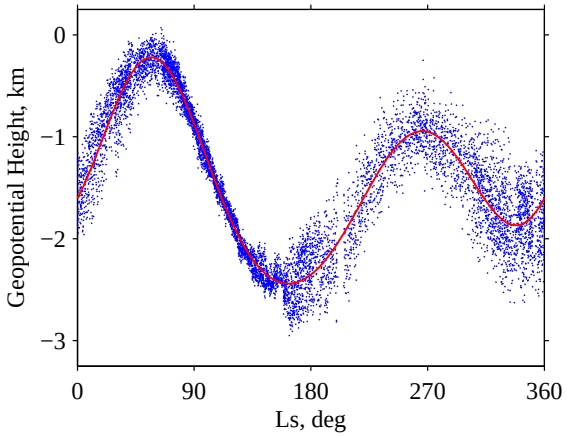

Figure 2: Radio occultation measurements of geopotential height at 610 Pa. The figure contains data collected at high northern latitudes between $L_s = 270^\circ$ of Mars year 24 (MY 24) and $L_s = 270^\circ$ of MY 26. (In the convention used here MY 1 begins at $L_s = 0^\circ$ on April 11, 1955.) The smooth curve shows an empirical model for the seasonal variations.

Introduction: Radio occultation experiments were conducted routinely with Mars Global Surveyor (MGS) between January 1998 and September 2006, a span of about 4.5 Martian years, yielding more than 21,000 profiles of the neutral atmosphere. These experiments have sampled the atmospheric structure at essentially all latitudes on Mars at one season or another, as shown in Figure 1, with uniform coverage in longitude. The distribution of the measurements in longitude, latitude, and season is well suited to focused investigations of planetary-scale dynamics, such as transient eddies [1,2], thermal tides [3,4], and stationary Rossby waves [5,6].

Each MGS occultation experiment yields a profile of temperature T and pressure p versus radius that extends from the surface to a pressure of about 10 Pa, corresponding to an altitude of about 40 km in the tropics [7,8,9]. The uncertainties in T and p vary strongly with pressure, decreasing from about 5% at 10 Pa to about 0.3% at 610 Pa, near the surface. The radius scale inherent in each profile has an uncertainty of a few meters, commensurate with the accuracy of the MGS orbit reconstructions [10]. This allows accurate registration of the retrieved profiles within the gravity field of Mars and provides a unique measure of geopotential height Z on surfaces of constant pressure. The uncertainty in p limits the accuracy of Z to about 30 m at 610 Pa. These profiles are available from both PDS and a more versatile MGS Radio Science web site (http://nova.stanford.edu/projects/mgs/).

This discussion focuses on occultation measurements of geopotential height. The sections that follow describe recent results concerning baroclinic eddies [2] and Kelvin waves [4].

Baroclinic Eddies: MGS radio occultations provide a valuable record of variations in Z on time scales from diurnal to interannual. For example, Figure 2 shows results at 610 Pa from a series of about 8700 experiments spanning 2 Mars years. Within the latitude range of these measurements, 55°–85°N, the average surface elevation is about −4 km, so that the 610 Pa pressure level is generally a few kilometers above the surface. The measurements are distributed uniformly in longitude. At this pressure level, the uncertainty in Z is typically about 30 m, barely discernible on the scale of Figure 2.

The geopotential height at 610 Pa, Z_{610}, varies gradually with season by more than 2 km. This arises from several sources, including seasonal condensation and sublimation of carbon dioxide, seasonal evolution of the planetary-scale circulation, and the thermal expansion and contraction of the lowest few kilometers of the atmosphere, which also varies systematically with season. The smooth curve in Figure 2 is an empirical model for the annual cycle of Z_{610}, as derived through Fourier analysis of the data.

The fluctuations of Z_{610} about the seasonal trend in Figure 2 are caused primarily by baroclinic eddies, with a weaker contribution from stationary Rossby waves, and their properties vary strongly with season. As an example, Figure 3 characterizes the wave activity during early winter ($L_s = 270^\circ$–285°) at 62°N. This is the spectrum of variations in Z_{610} as observed from the satellite frame at fixed local time. When viewed from this frame the frequency f of an atmospheric wave is Doppler shifted due to rotation of Mars, so that the spectrum measures the combined effects of zonal and temporal variations. This

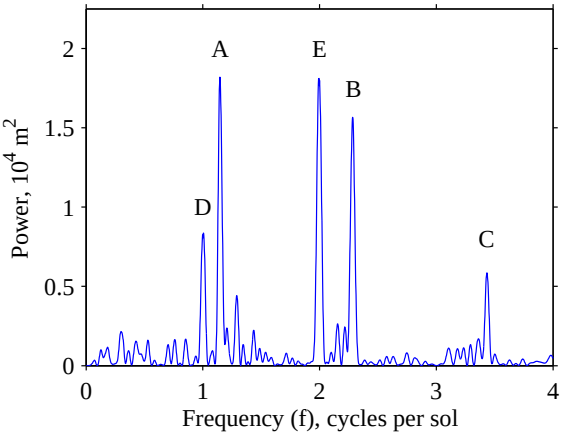

Figure 3: Power spectrum of eddy activity at 62°N. These results were obtained from observations of Z_{610} during L_s = 270°–285° of MY 24.

can be expressed as

$$f = \sigma + s/\Delta\,, \qquad (1)$$

where σ is the wave frequency as observed from the surface, s is the zonal wave number (dimensionless), and Δ is the mean solar day (1 sol = 88,775 s). Observations of f, such as those in Figure 3, constrain the values of σ and s but do not define them uniquely. With guidance from previous observations, such as Viking Lander measurements of σ, it is generally possible to resolve this ambiguity.

The spectrum in Figure 3 contains five prominent peaks. Of these, three are transient eddies and two are stationary waves. The transient eddies appear at (A) $f = 1.15$ sol^{-1} corresponding to $s = 1, \sigma = 0.15$ sol^{-1}, and a period $P = 6.8$ sols, (B) $f = 2.28$ sol^{-1} corresponding to $s = 2$, $\sigma = 0.28$ sol^{-1}, and $P = 3.5$ sols, and (C) $f = 3.43$ sol^{-1} corresponding to $s = 3$, $\sigma = 0.43$ sol^{-1}, and $P = 2.3$ sols. All three modes travel eastward with a zonal phase speed of about 52° sol^{-1}. The spectral peaks at (D) $f = 1.0$ sol^{-1} and (E) $f = 2.0$ sol^{-1} are stationary waves with $s = 1$, $\sigma = 0$ sol^{-1} and $s = 2$, $\sigma = 0$ sol^{-1}, respectively. Space-time analysis also yields least-squares solutions for the amplitude of each mode [2].

Hinson [2] characterized the seasonal evolution of transient eddies in the northern hemisphere by applying this method of analysis to all data in Figure 2. According to these occultation measurements, the "weather" in the lowest scale height above the surface at high northern latitudes is dominated by shallow, intense, eastward-moving baroclinic eddies. Eddy activity appears as well-defined modes with s = 1–3, and variations in the amplitudes of these modes tend to be anticorrelated so that a large amplitude in one mode is often accompanied by a small amplitude in the others. The wave number and period of the dominant mode shift at intervals of 30–50 sols. These results evoke the distinctive "baroclinic wave transitions" that appear in pressure measurements by Viking Lander 2 [11],

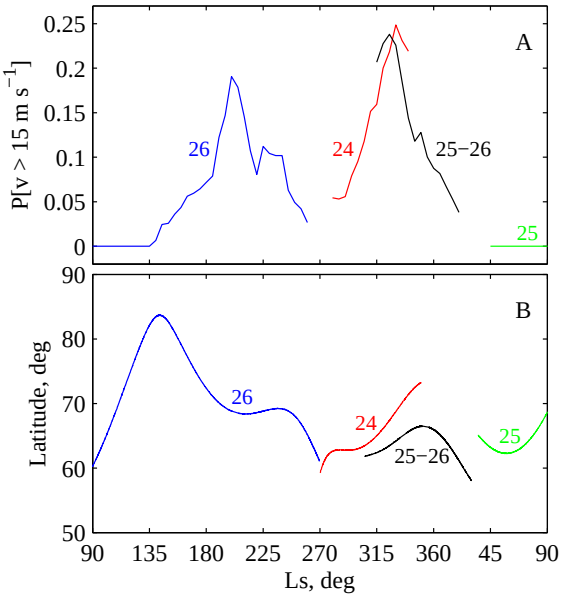

Figure 4: Seasonal variations of meridional wind speed at 610 Pa. (a) Fraction of wind samples whose magnitude exceeds 15 m s^{-1} from within a sliding 20° window of L_s. (b) Latitude of measurements, which varies gradually with season. The numbers adjacent to the curves in both panels refer to the Mars year of the observations.

and the two sets of observations provide highly complementary characterizations of eddy behavior [12,13].

The occultation measurements of Z_{610} in Figure 2 were also used to investigate eddy-driven meridional winds near the surface [2], where estimates of wind speeds are extremely sparse. At 610 Pa, the flow is decoupled from surface friction (in the latitude range considered here) and the Rossby number is relatively small. The meridional wind speed is then proportional to the zonal gradient of Z_{610}.

Occultations conducted on consecutive orbits of MGS yield values of Z_{610} at fixed latitude but the measurements are not simultaneous. During the interval of 0.08 sols between each pair of observations, the measurement longitude moves westward by about 29° while the transient eddies travel eastward by about 4°. Hence the effective zonal separation of the measurements is about 33°. Apart from this small correction for eddy motion, the meridional wind speed can be obtained with little difficulty, requiring no other assumptions about the period or zonal wave number of the eddies.

Estimates of the meridional wind speed were derived from the measurements in Figure 2 for all cases where data are available from successive orbits, yielding about 6600 wind samples over a span of 2 Mars years [2]. It is convenient to express the results as a distribution function. For example, Figure 4 shows the fraction of wind speeds that exceeds 15 m s^{-1} computed from data within a sliding 20° window of L_s. Wind speeds in the tail of the distribution function, which reach 30 m s^{-1} at 610 Pa in midwinter, are particularly important

because of their potential to raise dust from the surface.

The eddy winds in Figure 4a vary distinctively with season in response to changes in eddy amplitude and zonal wave number [2]. The meridional winds peak sharply in two seasonal windows, one in early-to-middle autumn and another in middle-to-late winter, separated by a lull around winter solstice. The strongest winds occur in midwinter in connection with intense wave-3 eddies with a period of about 2.3 sols. These results reinforce key conclusions drawn from other MGS observations.

The MGS Mars Orbiter Camera (MOC) is systematically mapping the seasonal and spatial distributions, intensity, and morphology of Martian dust storms. On some occasions dust storms appear in the form of nearly linear dust fronts that travel southward from high northern latitudes into the tropics [14,15]. The most intense events of this sort occur within two seasonal windows, early-to-middle autumn ($L_s = 200°$–$240°$) and middle-to-late winter ($L_s = 310°$–$350°$), while the interval surrounding winter solstice is devoid of such activity [16,17]. These frontal dust storms are initiated by eastward traveling baroclinic eddies, especially wave-3 modes with periods of 2–3 sols [16,17]. Simulations by Mars General Circulation Models (MGCMs) support this conclusion [15,18], and also indicate that interactions among transient eddies, thermal tides, and western boundary currents strongly influence the development and evolution of frontal dust storms and their capacity to transport dust to low latitudes.

In summary, the baroclinic eddies of the northern hemisphere contribute to the characteristic seasonal variations in tropical dust opacity. The mechanism that controls the intensity and zonal wave number of the dominant eddies indirectly modulates the seasonal dust cycle and hence the climate of Mars.

Subsequent to the publication of the results reviewed here [2], MGS acquired additional occultation measurements at high latitudes in both the northern and southern hemispheres. These data will enable further investigations of baroclinic eddies. Important aspects of eddy behavior remain unexplained, including the striking hemispheric asymmetry in eddy activity and the occurrence of distinctive "storm zones" of enhanced eddy activity in both hemispheres.

Kelvin Waves: *Hinson et al.* [4] recently analyzed data from a series of radio occultation experiments conducted concurrently with MGS and Mars Express (MEX) in mid-2004. The season on Mars was midspring of MY 27 ($L_s = 35°$–$70°$). They supplemented the observations with numerical simulations by the MGCM of the Geophysical Fluid Dynamics Laboratory [19]. At tropical latitudes, the geopotential field derived from these measurements contains distinctive zonal modulation caused by solar-asynchronous thermal tides. This combination of observations and simulations allows both diurnal and semidiurnal Kelvin waves to be identified with confidence. The resulting characterization of the wave-2 semidiurnal Kelvin wave is more complete and less ambiguous than any previous measurement. The well-known wave-1 diurnal Kelvin wave (DK1) is the dominant solar-asynchronous tide in the Martian atmosphere, and the results derived from these

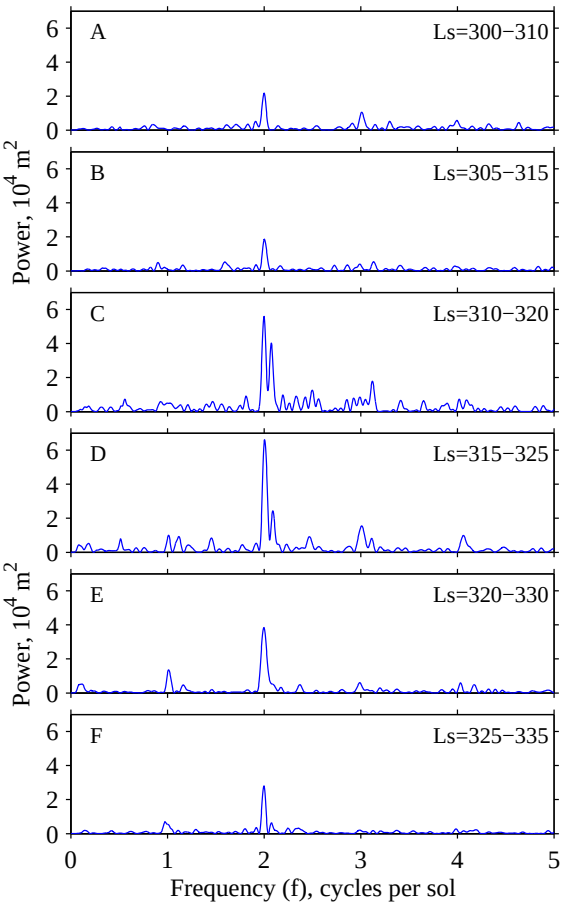

Figure 5: Power spectra of geopotential height at 200 Pa from MGS occultation measurements at low latitudes during northern winter of MY 26.

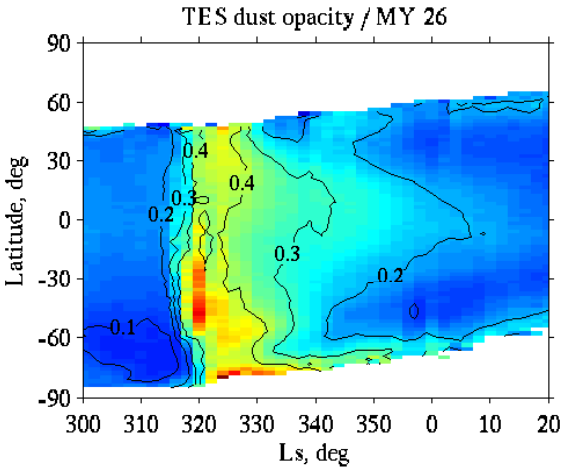

Figure 6: Zonally averaged dust opacity measured by the MGS TES during northern winter of MY 26 [20]. A substantial dust storm caused the opacity to increase sharply between $L_s = 315°$ and $L_s = 320°$.

occultation data confirm and extend previous observations by diverse instruments.

The DK1 produces strong modulation at $f = 2.0$ sol^{-1} in occultation measurements of Z. For example, Figure 5 shows results from a series of MGS occultations at low latitudes during northern winter of MY 26. The DK1 is the dominant mode in each spectrum of this sequence, which tracks its evolution during the rapid growth and gradual decay of a substantial dust storm. Figure 6 shows the dust opacity during this interval as measured by the MGS Thermal Emission Spectrometer (TES) [20].

The DK1 has a moderate amplitude when the dust opacity is relatively small, prior to $L_s = 315^\circ$ (Figures 5a and 5b). It intensifies sharply during the initial rapid growth in dust opacity (Figure 5c), and its peak amplitude coincides roughly with the peak in dust opacity near $L_s = 320^\circ$ (Figure 5d). The amplitude of the DK1 returns to about its pre-dust storm level at $L_s = 330^\circ$ (Figure 5f). The dust opacity at $L_s = 330^\circ$ is still elevated, as shown in Figure 6, but its distribution is probably more zonally uniform than in the early phase of this dust storm, which may reduce its impact on the DK1. Note that the spectra in Figures 5c and 5d resolve a strong spectral peak at about $f = 2.08$ sol^{-1}, possibly associated with particularly intense baroclinic eddies that contribute to the initiation of this dust storm [17], as discussed in the previous section.

The observations in Figures 5 and 6 are the subject of an ongoing investigation.

References:

[1] Hinson, D. P., and R. J. Wilson (2002), Transient eddies in the southern hemisphere of Mars, *Geophys. Res. Lett., 29*, 1154, doi:10.1029/2001GL014103.

[2] Hinson, D. P. (2006), Radio occultation measurements of transient eddies in the northern hemisphere of Mars, *J. Geophys. Res., 111*, E05002, doi:10.1029/2005JE002612.

[3] Hinson, D. P., and R. J. Wilson (2004), Temperature inversions, thermal tides, and water ice clouds in the Martian tropics, *J. Geophys. Res., 109*, E01002, doi:10.1029/-2003JE002129.

[4] Hinson, D. P., M. Pätzold, R. J. Wilson, B. Häusler, S. Tellmann, and G. L. Tyler (2007), Radio occultation measurements and MGCM simulations of Kelvin waves on Mars, *Icarus*, submitted.

[5] Hinson, D. P., G. L. Tyler, J. L. Hollingsworth, and R. J. Wilson (2001), Radio occultation measurements of forced atmospheric waves on Mars, *J. Geophys. Res., 106*, 1463–1480.

[6] Hinson, D. P., R. J. Wilson, M. D. Smith, and B. J. Conrath (2003), Stationary planetary waves in the atmosphere of Mars during southern winter, *J. Geophys. Res., 108*, 5004, doi:10.1029/2002JE001949.

[7] Hinson, D. P., R. A. Simpson, J. D. Twicken, G. L. Tyler, and F. M. Flasar (1999), Initial results from radio occultation measurements with Mars Global Surveyor, *J. Geophys. Res., 104*, 26,997–27,012.

[8] Hinson, D. P., M. D. Smith, and B. J. Conrath (2004). Comparison of atmospheric temperatures obtained through infrared sounding and radio occultation by MGS, *J. Geophys. Res., 109*, E12002, doi:10.1029/2004JE002344.

[9] Tyler, G. L., G. Balmino, D. P. Hinson, W. L. Sjogren, D. E. Smith, R. A. Simpson, S. W. Asmar, P. Priest, and J. D. Twicken (2001), Radio Science observations with Mars Global Surveyor: Orbit insertion through one Mars year in mapping orbit, *J. Geophys. Res., 106*, 23,327–23,348.

[10] Lemoine, F. G., D. E. Smith, D. D. Rowlands, M. T. Zuber, G. A. Neumann, D. S. Chinn, D. E. Pavlis (2001), An improved solution of the gravity field of Mars (GMM-2B) from Mars Global Surveyor, *J. Geophys. Res., 106*, 23,359–23,376.

[11] Collins, M., S. R. Lewis, P. L. Read, and F. Hourdin (1996), Baroclinic wave transitions in the Martian atmosphere, *Icarus, 120*, 344–357.

[12] Ryan, J. A., and R. D. Sharman (1981), Two major dust storms, one Mars year apart: Comparison from Viking data, *J. Geophys. Res., 86*, 3247–3254.

[13] Barnes, J. R. (1981), Midlatitude disturbances in the Martian atmosphere: A second Mars year, *J. Atmos. Sci., 38*, 225–234.

[14] Cantor, B. A., P. B. James, M. Caplinger, and M. J. Wolff (2001), Martian dust storms: 1999 Mars Orbiter Camera observations, *J. Geophys. Res., 106*, 23,653–23,687.

[15] Wang, H., M. I. Richardson, R. J. Wilson, A. P. Ingersoll, A. D. Toigo, and R. W. Zurek (2003), Cyclones, tides, and the origin of a cross-equatorial dust storm on Mars, *Geophys. Res. Lett., 30*, 1488, doi:10.1029/2002GL016828.

[16] Wang, H., R. W. Zurek, and M. I. Richardson (2005), Relationship between frontal dust storms and transient eddy activity in the northern hemisphere of Mars as observed by MGS, *J. Geophys. Res., 110*, E07005, doi:10.1029/2005JE002423.

[17] Wang, H. (2007), Dust storms originating in the northern hemisphere during the third mapping year of Mars Global Surveyor, *Icarus, in press*, doi:10.1016/j.icarus.2007.01.014.

[18] Newman, C. E., S. R. Lewis, P. L. Read, and F. Forget (2002), Modeling the Martian dust cycle: 2. Multiannual radiatively active dust transport simulations, *J. Geophys. Res., 107*, 5124, doi:10.1029/2002JE001920.

[19] Wilson, R. J., and K. Hamilton (1996), Comprehensive model simulation of thermal tides in the Martian atmosphere, *J. Atmos. Sci., 53*, 1290–1326.

[20] Smith, M. D. (2004), Interannual variability in TES atmospheric observations of Mars during 1999–2003, *Icarus, 167*, 148–165.